Article

Gas Mass-Transport Coefficients in Ionomer Membranes Using a Microelectrode

John G. Petrovick, Clayton J. Radke, and Adam Z. Weber*

Read Online

ACCESS | 📊 Metrics & More | 📖 Article Recommendations | 🗐 Supporting Information

ABSTRACT: Gas permeability, the product of gas diffusivity and Henry's gas-absorption constant, of ionomer membranes is an important transport parameter in fuel cell and electrolyzer research as it governs gas crossover between electrodes and perhaps in the catalyst layers as well. During transient operation, it is important to divide the gas permeability into its constituent properties as they are individually important. Although transient microelectrode measurements have been used previously to separate the gas permeability into these two parameters, inconsistencies remain in the interpretation of the experimental techniques. In this work, a new interpretation methodology is introduced for determining independently diffusivity and Henry's constant of hydrogen and oxygen gases in ionomer membranes (Nafion 211 and Nafion XL) as a function of relative humidity using microelectrodes. Two time regimes are accounted for. At long times, gas permeability is determined from a two-dimensional numerical model that calculates the solubilized-gas concentration profiles at a steady state. At short times, permeability is deconvoluted into diffusivity and Henry's constant by analyzing transient data with an extended Cottrell equation that corrects for actual electrode surface area. Gas permeability and diffusivity increase as relative humidity increases for both gases in both membranes, whereas Henry's constants for both gases decrease with increasing relative humidity. In addition, results for Nafion 211 membranes are compared to a simple phase-separated parallel-diffusion transport theory with good agreement. The two-time-regime analysis and the experimental methodology can be applied to other electrochemical systems to enable greater precision in the calculation of transport parameters and to further understanding of gas transport in fuel cells and electrolyzers.
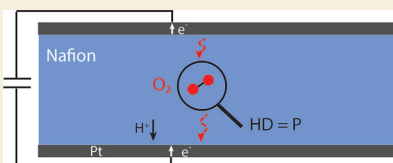
KEYWORDS: *permeability, diffusivity, Henry's constant, Nafion, Cottrell equation, chronoamperometry, rough electrode surface*

INTRODUCTION

Polymer-electrolyte fuel cells (PEFCs) are a critical next-generation renewable energy technology due to their potential to replace traditional internal combustion engines in both light- and heavy-duty transportation. PEFCs operate through the conversion of hydrogen and oxygen gases to water vapor via hydrogen-oxidation (HOR) and oxygen-reduction (ORR) reactions. These reactions occur at the anode and cathode catalyst layers, respectively, and are separated by an ion-conducting polymer (ionomer). As a result, crossover of gases, specifically hydrogen and oxygen, through the ionomer membrane is deleterious and a significant contributor to PEFC inefficiencies as the movement of hydrogen and/or oxygen to opposing electrodes can result in Pt degradation and mixed potentials.[1,2] Ionomer thin films also act as a binder and ion conductor in the catalyst layers to hold together agglomerates of platinum (Pt) catalyst supported on carbon particles; it has been shown that oxygen transport through these films can limit fuel cell performance.[3,4] The gas permeability of the membrane or thin film captures gas transport under steady-state conditions.[5] However, fuel cells do not solely operate at steady state. In applications such as heavy-duty trucks, power loads vary due to both normal operation and fuel cell degradation.[6−8] Thus, the individual

parameters permeability, diffusivity, and Henry's constant are necessary to capture fully the transient fuel cell performance.[5]
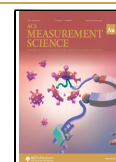
The most common PEFC ionomer is Nafion, a perfluorosulfonic acid (PFSA) polymer. It consists of a hydrophobic fluorinated polyethylene backbone with ether-fluorocarbon side chains that terminate in hydrophilic sulfonic acid groups (the molecular structure of Nafion is given in Section S1.1, Figure S1 of the Supporting Information).[1] PFSA ionomers are phase-separated with discrete polymer- and water-filled domains and are typically categorized by their equivalent weight (EW) or grams of dry polymer per mole of ionic group.[1] Several different models for the microstructural phase separation in Nafion have been proposed, including the cluster-network model by Hsu and Gierke[9] and the ribbon model by Kreuer and Portale,[10] as have been reviewed and discussed by Kusoglu and Weber[1] and Mauritz and Moore.[11] However, for the present analysis, a simple phase-separated parallel-channel model captures the impact of water content on the effective

ACS Publications
© 2022 The Authors. Published by
American Chemical Society
208
https://doi.org/10.1021/acsmeasuresciau.1c00058
ACS Meas. Sci. Au 2022, 2, 208−218

gas-transport properties, as discussed below. The atomistic microstructure can also be influenced by the surface Nafion is coated on, including the presence of lamellae as discussed in the literature,[12−15] although such nanoscopic details are averaged in our analysis as part of the membrane and catalyst system.

The diffusivity, Henry's constant, and permeability of oxygen gas in Nafion membranes are well-studied.[16−22] Conversely, hydrogen gas is less well-studied, with a primary focus on permeability in-lieu of individual diffusivity and Henry's constant.[19,23−25] There are several methods of interrogating gas-transport properties, including gas crossover, electrochemical monitoring, and permeation experiments.[16,17,24,26] The apparatus discussed here is a microelectrode, traditionally defined as an electrode smaller than 100 μm in lateral dimension.[27] The primary advantages of microelectrodes are the well-defined working electrode area and extremely low current draw that allow the ohmic potential drop to remain small even when working with relatively high-resistance electrolytes such as solid-state ionomers.[28] In addition, the apparatus acts as a mimic for the environment found in a PEFC, as the electrode can be exposed to the same electrolyte, potential, humidity, and gases as in a functioning PEFC, but in a much more controlled manner.[28] This gives microelectrode assemblies a distinct advantage over traditional aqueous electrolyte techniques, such as rotating disk electrodes (RDEs), when studying PEFC electrochemistry.[28]

A typical microelectrode assemblage features a microelectrode pressed into contact with an ionomer membrane with the entire chamber exposed to humidified reactant gases. Here, the electrostatic potential difference is adjusted to attain the limiting-current regime. Once limiting-current conditions are met, current decay is recorded as a function of time. Current history is then fit by mathematical expressions, such as those of Cottrell or Shoup−Szabo, to determine diffusivity and Henry's constant.[21] The governing mathematical expressions have been rigorously studied for aqueous electrolytes (equivalent to infinitely thick membranes in our microelectrode), notably by the work of Zoski et al.[29] However, our membranes are of finite thickness, requiring more a detailed analysis, as we have done for the first time.

Despite the large effort invested, questions linger about quantitative gas-transport values so obtained.[16,17,19−22,26,30−34] Most works follow the same general experimental procedure, discussed in the previous paragraph, involving chronoamperometry performed under limiting-current conditions. Disagreements arise with the analysis of the data, including what equations to use and where to apply them. First, there is disagreement over the interpretation methodology. The original work by Parthasarathy et al. advocated the Cottrell equation, whereas Chlistunoff used the Shoup−Szabo equation, and Novitski et al. recommended using only a numerical model, discarding analytical solutions entirely.[20,31,35] In the latter case, deviations of up to approximately 30% between the analytical and numerical models are reported.[31] Second, the time range utilized for fitting the adopted equations to experimental data varies widely. Parthasarathy et al. used a large time range of up to ∼20 s, whereas Novitski et al. fitted a linear section in the ms regime, and Chlistunoff concluded that no longer than ∼10 s should be exercised. Although general trends remain similar between these analysis techniques, the values of oxygen mass-transport parameters can vary by over an order of magnitude among various studies,

even for very similar experimental systems and membranes.[20−22] Finally, some studies report anomalous deviations from expected currents at very short time scales.[33]

In this work, an improved methodology is developed for interpreting the current-time curves at mass-transport limiting current. The procedure ensures high precision by analyzing short-time and long-time current asymptotes, rather than relying only on short-time measurements. A rigorous two-dimensional (2D) diffusion model describes the long-time steady behavior in a finite-thickness membrane, while a surface-roughness-extended Cottrell expression accounts for short times. Our proposed analysis method is applied to ionomer membranes of Nafion 211 and Nafion XL, a polytetrafluoroethylene-reinforced variant of Nafion. The gas diffusivity, Henry's constant, and permeability are presented for both hydrogen and oxygen gases as functions of relative humidity. Finally, a simple phase-separated parallel-diffusion model explores the experimental results for Nafion 211, allowing for greater insight into the physical transport processes occurring within PFSA ionomers.

■ EXPERIMENTAL METHODS

Microelectrode Cell Design

The experimental microelectrode cell has been described previously.[36] A schematic is provided in Figure 1. In brief, the cell is a two-
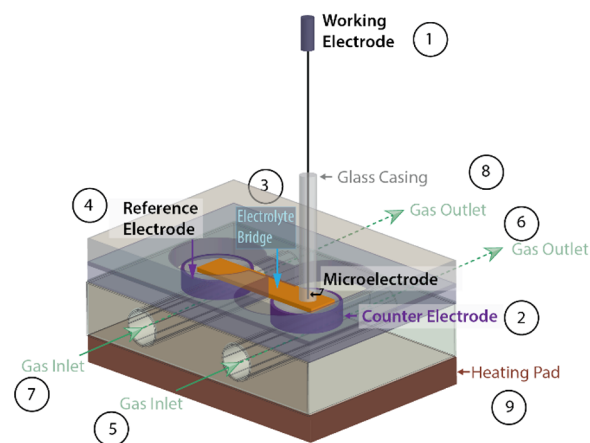

Figure 1. Schematic of the microelectrode cell. Electrodes are labeled (1), (2), and (4), while the electrolyte resides near (3). Gas enters through inlets (5 and 7), flows in-plane through the gas diffusion electrodes with minimal resistance, and exits through the outlets (6 and 8). A heating pad (9) sits beneath the cell but is unused in this work.

chambered, flow-through design with one chamber containing the working (micro-) and counter electrodes and one for a reversible hydrogen (RHE) reference electrode. The two chambers were sealed but were connected by a salt bridge of the ionomer of interest (e.g., Nafion 211), which also serves as the electrolyte separating the working and counter electrodes. Gas was humidified before entering the cell, and each chamber's gas flow was controlled independently. To ensure good contact between the working electrode and the membrane, a fine-threaded screw applied mechanical force to the top of the working electrode, as measured by a resistive pressure sensor. To prevent leakage of reactive gases directly to the electrode surface (thereby bypassing the membrane), a Nafion adhesion layer was first dropcast on the microelectrode prior to cell construction by placing a single drop of D2021 Nafion dispersion (Ion Power, Delaware, USA) on the microelectrode tip. The cell was wrapped in a Faraday cage of aluminum foil to limit electrical noise.
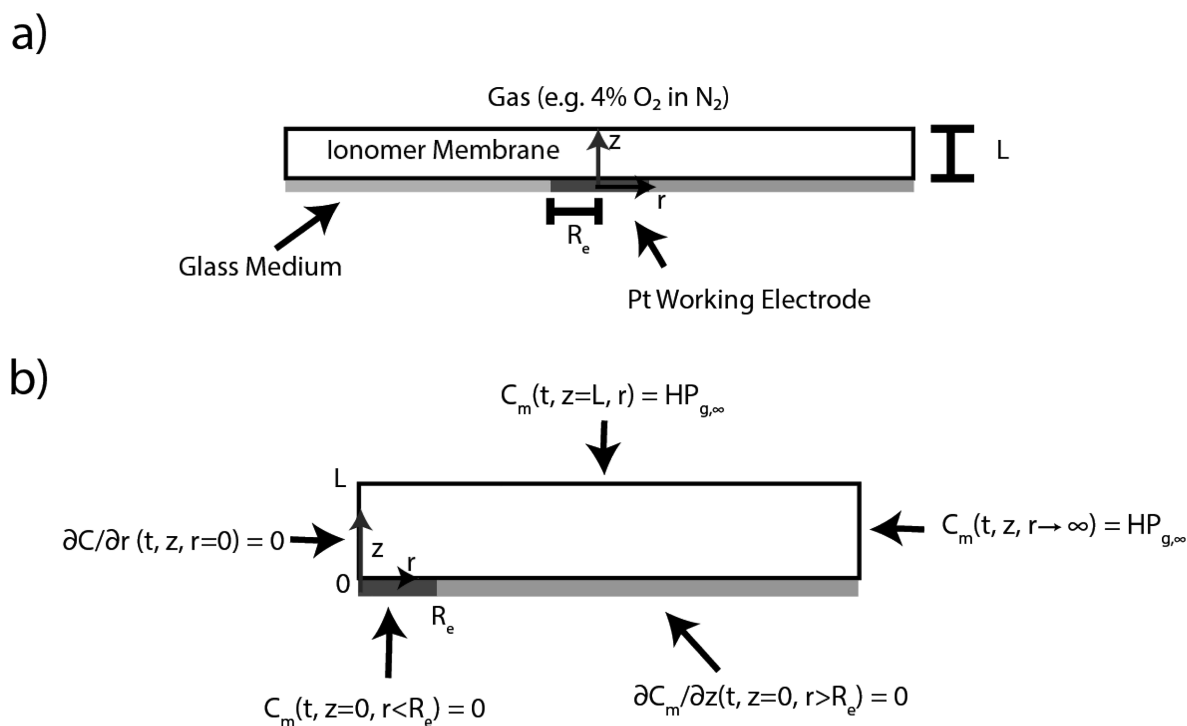
a)

b)

Figure 2. (a) Schematic of electrode geometry in the microelectrode. (b) Schematic of the calculation domain labeling the boundary conditions for the microelectrode, except for the initial condition $C_m(0, z, r) = HP_{g,\infty}$.

Materials

The microelectrode cell was fabricated from inert polyether ether ketone (PEEK) (McMaster-Carr, Illinois, USA). A 50 μm Pt microelectrode (BASi, Inc., Indiana, USA, polished sequentially using 15 μm diamond, 3 μm diamond, 1 μm alumina, and 0.05 μm alumina powder, rinsed with DI water to remove contaminants, and dried under a N_2 stream) is the primary working electrode, whereas the counter and reference electrodes are Pt-coated gas-diffusion electrodes (GDEs) (Sigracet 25 BC, 0.5 mg/cm^2 Pt, SGL Carbon, Wiesbaden, Germany). The two membrane types used were Nafion 211 (25 μm, 1100 EW, preboiled, Ion Power, Delaware, USA) and Nafion XL (~28 μm, 1100 EW, as-received, Ion Power, Delaware, USA). Both are proton-exchange membranes. In addition, Nafion XL is reinforced with an ~3 μm polytetrafluoroethylene layer for additional mechanical stability.[37] Water uptake and swelling profiles account for the change of membrane thickness with humidity.[1,37] Gases used were argon (Praxair, Connecticut, USA), hydrogen (Praxair, Connecticut, USA, 2% in argon), and oxygen (Airgas, Pennsylvania, USA, 4% in nitrogen).

Atomic force microscopy (AFM) was performed on a bare Pt microelectrode with a Bruker (Massachusetts, USA) AFM probe over a scanning window of 10 μm × 10 μm. The open-source Gwyddion software package (Czech Metrology Institute, Czech Republic) performed post-processing and analyzed the AFM images.

Electrochemical Surface Area

Cyclic voltammetry (CV) ascertained the electrochemical surface area (ECSA) of the microelectrode surface by evaluating the area of the hydrogen underpotential-deposition region.[28] In this method, the peaks appearing in the approximate range of 0−0.4 V on the CV scan represent hydrogen desorption and adsorption depending on whether the current is positive or negative, respectively.[27] By integrating the area under the desorption peak, subtracting the double-layer capacitance region, and dividing by the scan rate, the total adsorbed charge from this process can be determined. By assuming that hydrogen adsorbs in a monolayer with a surface charge density of 210 μC/cm^2,[27] the electrochemical surface area is calculated by[21]

$$ECSA = \frac{A_{UC}}{\nu \rho_s} \tag{1}$$

where ECSA is the electrochemical surface area, A_{UC} is the area under the curve [A·V], ν is the scan rate [V/s], and ρ_s is the surface charge density [C/cm^2]. The roughness factor, R_F, is then defined as ECSA divided by the geometric area. Details are given in Section S1.2 in the Supporting Information. CV curves were recorded under argon gas at room temperature and 90% relative humidity (RH) at a scan rate of 50 mV/s. Three CVs were recorded with high reproducibility, with the surface area calculated from either cycle 2 or 3, depending on feature clarity. Prior to the recorded CVs, 50 sequential CVs were performed at a scan rate of 500 mV/s to clean the surface. A typical CV scan is given in Figure S2 of the Supporting Information with the pertinent integrated area highlighted. R_F values varied depending on the specific electrode in use but ranged from 4.3 to 14.8.

Electrochemical Techniques

Chronoamperometry was used to determine the mass-transport coefficients of oxygen and hydrogen in the ionomer membranes.[27] Prior to measurement, the microelectrode cell was held at open-circuit voltage (OCV) for 10 min, until no significant change in OCV with time was observed. The potential was then set to 0.5 V versus OCV and −0.7 V versus OCV for hydrogen and oxygen, respectively, where the specific values were predetermined from identifying the mass-transport limit in obtained polarization curves (see Figure S3a and Figure S3b for ORR and HOR, respectively, in Section S1.3 of the Supporting Information). Potentials were held at those values for 5 min with the transient current recorded every 100 ms using an SP-300 potentiostat (Bio-Logic, Seyssinet-Pariset, France) equipped with an ultralow current precision channel. The humidity of each chamber was controlled either by external humidifiers (Humidification System, Fuel Cell Technologies, New Mexico, USA) or by a custom wet/dry gas mixing bubbler and varied depending on the particular membrane under study to capture an effective range of relative humidities. Nafion 211 was tested at 25, 60, 75, 85, and 95% RH. Nafion XL was tested at 30, 60, 75, 85, and 90% RH. All measurements were performed at room temperature, approximately 20 °C.

Hydrogen is classified as a GHS flammable gas, category 1. To stay below the flammability limit, 4% or less hydrogen (balance argon) was used.

■ THEORY

2D Numerical Solution for the Transient Current

Gas diffusion to the surface of the microelectrode through the ionomer membrane is the subject of several previous studies.[20−22,33,34] In most works, however, a modified Cottrell equation fits the current transient to extract gas diffusivity and Henry's constant.[28] The modified Cottrell equation describes the mass-transport limiting-current density at a planar electrode in a semi-infinite electrolyte as a function of time.[20] A typical form for use with disk electrodes of radius R_e is[20]

$$I = \frac{(nF\pi^{1/2}R_e^2 D^{1/2} H P_{g,\infty})}{\sqrt{t}} + \pi n F D H P_{g,\infty} R_e \tag{2}$$

where I is the current, n is the number of electrons transferred, F is Faraday's constant (96,485 C/mol), D is the effective membrane gas diffusivity, $P_{g,\infty}$ is the set external gas partial pressure, H is the effective Henry's constant, and t is the time.[20] The first term on the right of eq 2 corresponds to transient growth of a diffusion boundary layer in a stagnant infinite medium, while the second term is empirically added to describe the steady-state current to a finite radius disk in an infinite electrolyte. However, an infinite-thickness membrane is not achievable in a microelectrode cell where the membrane thickness is on the same order as the electrode size, rendering the accuracy of the steady-state term questionable. In addition, the first term on the right of eq 2 is restricted to short times only, where the boundary of the diffusion field has not reached the thickness of the membrane; it is not clear at what precise time this condition is met.

To alleviate the finite membrane thickness approximation in eq 2, a 2D numerical model was implemented based on molecular diffusion through the membrane. Figure 2a illustrates the system geometry. A finite-radius flat disk electrode of radius R_e is embedded in an impermeable substrate that extends infinitely in the r dimension. The infinite-radius ionomer membrane rests on this surface and extends in the z direction to a distance L, the thickness of the membrane. The system is symmetric in the azimuthal coordinate. This geometry demands 2D transient diffusion in cylindrical coordinates

$$\frac{\partial C_m}{\partial t} = D\left[\frac{1}{r}\frac{\partial}{\partial r}\left(r\frac{\partial C_m}{dr}\right) + \frac{\partial^2 C_m}{\partial z^2}\right] \tag{3}$$

where r is the radial coordinate, z is the axial coordinate, and C_m is the gas concentration per unit volume of membrane. To solve this equation, four boundary conditions and one initial condition are required

$$\left[C_m\left(t, r < R_e, z = 0\right) = 0; \frac{\partial C_m}{\partial z}(t, r > R_e, z = 0) = 0\right]$$

$$\frac{\partial C_m}{\partial r}(t, r = 0, z) = 0; C_m(t, r = \infty, z) = H P_{g,\infty}$$

$$C_m(t, r, z = L) = H P_{g,\infty}; C_m(t = 0, r, z) = H P_{g,\infty} \tag{4}$$

In order, the boundary conditions correspond to zero surface concentration at the electrode due to the limiting current and zero surface flux in the surrounding impermeable glass medium (a piecewise boundary condition at $z = 0$), symmetry at the membrane center, constant equilibrium membrane concentration as r approaches infinity, constant equilibrium membrane concentration at the membrane finite-thickness boundary, and constant equilibrium concentration prior to the application of an electric potential. The fourth and fifth expressions state that the membrane exterior is in equilibrium with the external gas supply. Figure 2b delineates the boundary conditions.

At the surface of the electrode, the mass-transport-limited current is calculated from the expression

$$I(t) = -2\pi n F D \int_0^{R_e} \left[\frac{\partial C_m}{\partial z}(t, r, z = 0)\right] r\,dr \tag{5}$$

Upon nondimensionalizing C_m by $H P_{g,\infty}$, r by R_e, and z by L, eq 5 reduces at steady state to

$$I(t = \infty)$$
$$= -\pi n F D H P_{g,\infty} R_e \left[\frac{2R_e}{L} \int_0^1 \frac{\partial \tilde{C}_m}{\partial \tilde{z}}(\infty, \tilde{r}, 0)\tilde{r}\,d\tilde{r}\right] \tag{6}$$

where the over-squiggle symbol reflects nondimensional variables. The bracketed term on the right of eq 6 is a function only of the geometry. Accordingly, the steady finite-thickness current is not identical to the steady infinite-thickness current in eq 2. As in eq 2, however, only the product HD, or gas permeability, P, appears in eq 6. Thus, P is readily calculated by fitting eq 6 to the measured steady-state current. Once permeability is known, the measured transient current can then be fit to the transient solution of eq 5 to determine D (or H). Equations 3 and 4 (and thus the gradient in eq 5) are solved numerically in a finite-element multiphysics model, COMSOL 5.6. Numerical details (e.g., mesh density) can be found in Section S1.4 of the Supporting Information.

Either eqs 2 or 5 can be used to determine D, H, and P. Unfortunately, and not surprisingly, eqs 2 and 5 give disparate results for the same parameter values, as illustrated in Figure 3a. We find that the modified Cottrell equation (eq 2) deviates strongly from the finite-thickness numerical solution (eq 5) at long times and takes much longer to approach steady state. Both are consequences of a finite-thickness membrane in the numerical model compared to the infinite-thickness membrane in the modified Cottrell expression. A typical calculated steady-state profile from eq 5 is seen in Figure 3b. It is a flattened hemisphere due to the finite z boundary. The steady-state gas-concentration profile is clearly not one dimensional.

Figure 4 illustrates the application of eq 5 to typical experimental data for ORR from our microelectrode apparatus. Here, the permeability was fit using steady-state data and the
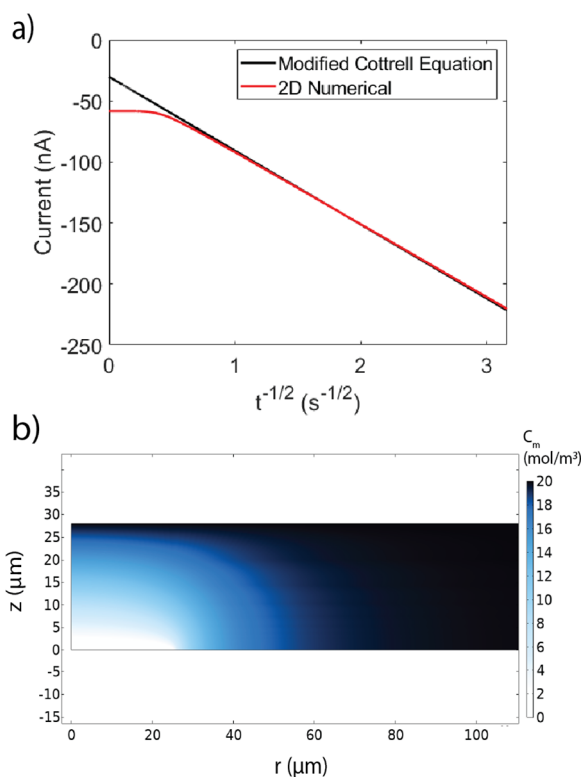
Figure 3. (a) Plot of current versus inverse square root of time comparing the modified Cottrell equation and the COMSOL solution using $D = 5 \times 10^{-11}$ m²/s, $H = 20$ mol/m³·bar, $L = 25$ μm, and $P_{g,\infty} = 1$ bar. (b) Concentration profile of oxygen gas in the system at a steady state, as calculated in COMSOL using $P_{g,\infty} = 1$ bar and $H = 20$ mol/m³·bar.
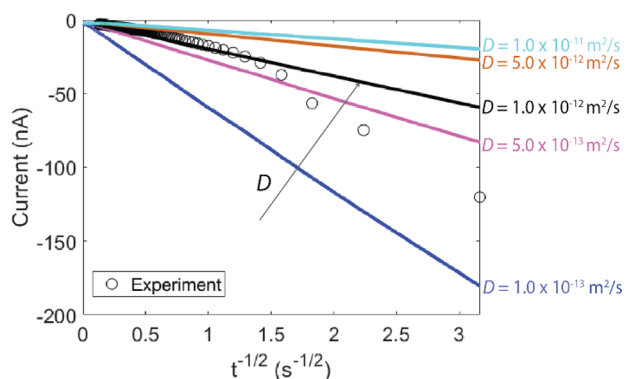

Figure 4. Comparison of eq 5 to typical ORR microelectrode experimental data. At low $t^{-1/2}$, the currents approach steady-state values of approximately −1 to −2 nA.

2D analysis in eqs 3 and 5 to 1.08×10^{-9} mol/(m·bar·s) and diffusivity was varied to fit the data. Adjustment of the oxygen-gas permeability allows eq 5 to show good agreement with the experiment at long times, as expected, but no matter the value chosen for diffusivity, the theory does not match the experimental short-time slope, as highlighted in Figure 4. A typical explanation for the deviation of eq 5 from the theory is double-layer charging, but based on electrode size and Nafion's RC (resistance-capacitance) constant,[30] charging effects should dissipate in the μs regime, whereas deviations from eq 5 clearly persist for up to 1 s ($t^{-1/2} > 1$) in Figure 4.

Rough Electrode Surface

An implicit assumption in eq 5 is that the electrode-reaction area is equal to the geometric area. However, even a polished Pt surface is not perfectly smooth.[21] We posit that the surface roughness of the Pt electrode should be accounted for (especially at short times) as it increases the initial available reactive area. A qualitative depiction of the hypothesized impact of the surface roughness on the current is illustrated in Figure 5a,b. At very short times, high concentrations of dissolved gas molecules in the previously equilibrated membrane reside directly in the rough Pt-electrode crevices. Because the diffusion boundary layer is initially infinitesimally thin, the rough surfaces appear locally planar, thereby increasing the electrode effective area (and therefore the current) compared to the flat geometric area used in the numerical model. As time increases, however, the diffusion layer grows, and gas molecules must travel from farther away in the membrane to reach the reactant surface. Here, the nanometer-size crevices of the electrode no longer contribute as much to the diffusion flux (the atomic-force micrograph of the microelectrode surface can be found in Figure S4 of the Supporting Information). Thus, the effective electrode-reaction area diminishes in time, approaching the physical geometric area. Changing area at short time is important when considering how to evaluate eq 5.

Chronoamperometric Data Interpretation

To provide meaningful estimates of membrane-gas diffusivities and Henry's constants, we propose a simple data-interpretation methodology. We suggest a two-time regime analysis. First, eq 6 is applied to calculate the gas permeability from the measured steady-state current and the geometric electrode area. Second, the short-time Cottrell equation is extended to account for surface roughness by the expression

$$ I = \frac{nF\pi^{0.5}PR_e^{2}P_{g,\infty}R_F}{D^{0.5}t^{0.5}} \tag{7} $$

with gas permeability defined by

$$ P = HD \tag{8} $$

where again R_F is the ECSA-determined roughness factor. All other variables are as defined previously.

Given the fitted experimental short-time slope, eq 7 permits assessment of the diffusion coefficient since permeability is known from fitting to eq 6. Henry's constant can then be determined from the definition of permeability in eq 8.

The advantage of this approach is that both steady-state and short-time information are used. Steady-state measurements yield accurate permeabilities, whereas roughness-corrected short-time data give meaningful diffusivities. It is assumed in the analysis that, for each measurement, water gradients are not present because measured currents are low and humidified gases are flowing. Thus, diffusivity and Henry's constant are taken to be constant for a given measurement and humidity. Discussion of the applicability of this analysis technique to experimental data can be found in the Results and Discussion section.

Phase-Separated Parallel-Diffusion Model

It is common to describe PFSA ionomers as composed of two distinct percolating phases when hydrated: a hydrophilic aqueous phase, consisting of tortuous water channels in the ionomer, and a hydrophobic polymer phase, consisting
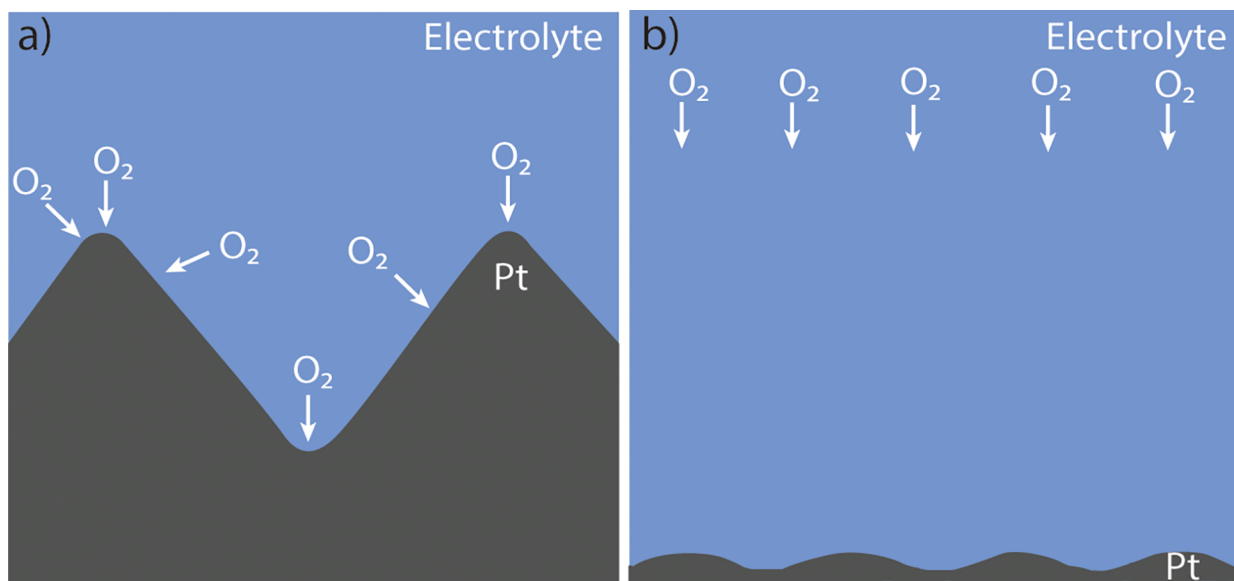
Figure 5. Accessible surface area for oxygen to react on the Pt surface at (a) very short time and (b) long time.

primarily of the polymer backbone.[1,38] Thus, to ascertain whether the suggested analysis procedure gives physically reasonable values for D, H, and P, a simple model was developed based on the assumption of phase separation of polymer and aqueous phases in the membrane. It is meant as a first-order rationalization of the results, described later, and is not intended to be a rigorous characterization of phase separation in Nafion membranes. This model is applied only to Nafion 211, as the addition of PTFE reinforcement in Nafion XL introduces multiple uncharacterized gas-transport pathways.[37] We assume further that diffusion is the only mode of mass transport. A mass balance on the diffusing gas in the membrane is

$$\varphi\frac{\partial c}{\partial t} + (1 - \varphi)\frac{\partial n}{\partial t} = \varphi D_a \nabla^2 c + (1 - \varphi)D_p \nabla^2 n_p \quad (9)$$

where c is the volume concentration of gas in the aqueous phase, n_p is the volume concentration of gas in the polymer phase, D_a is the diffusivity of the gas in the aqueous phase, D_p is the diffusivity of the gas in the polymer phase, and φ is the water volume fraction within the hydrated ionomer. Gas adsorption is neglected at the polymer/aqueous interface. By defining $C_m = \varphi c + (1 - \varphi)n$ (where C_m is the total gas concentration per volume of membrane) and assuming local equilibrium, such that the partition coefficient $K = n/c$, eq 9 can be rewritten as

$$\frac{\partial C_m}{\partial t} = D_{eff}\nabla^2 C_m \quad (10)$$

where

$$D_{eff} = \frac{D_a + D_p K(1 - \varphi)/\varphi}{1 + K(1 - \varphi)/\varphi} \quad (11)$$

Both aqueous and polymer phases are considered to have tortuous paths, so the diffusivities are modified from their bulk values[39−41]

$$D_a = D_a^\infty/\tau_a^2 \quad (12)$$

with

$$\tau_a^2 = e^{k/2(1/\varphi - 1)} \quad (13)$$

and

$$D_p = D_p^\infty/\tau_p^2 \quad (14)$$

with

$$\tau_p^2 = e^{k/2(1/(1-\varphi) - 1)} \quad (15)$$

where τ_a^2 and τ_p^2 are the tortuosities of the aqueous and polymer phases, respectively, and D_a^∞ and D_p^∞ are the diffusivities in bulk water and polymer, respectively. The porosity dependence of tortuosity follows from Yasuda *et al.* where k is a fitting parameter with a value of 0.93 (determined by Crothers *et al.*) for Nafion.[39,40] Similarly, the effective Henry's constant for the total membrane is a volume-average linear combination of the Henry's constants of each phase

$$H_{eff} = \varphi H_a + (1 - \varphi)H_p \quad (16)$$

where H_a represents Henry's constant for the aqueous phase, H_p is Henry's constant of the polymer phase, and $K \equiv H_p/H_a$. The product of eqs 11 and 16 is the gas permeability, P, of the ionomer membrane[22]

$$P \equiv D_{eff}H_{eff} \quad (17)$$

The phase-separation model predicts membrane diffusivity, Henry's constant, and permeability based on the diffusivity and Henry's constant of the gases in each of the individual phases and the overall membrane water content (volume fraction). By comparing the effective predicted values to the experimentally measured ones, physical insight can be made into the transport processes in the ionomer.

■ RESULTS AND DISCUSSION

Nafion 211

We argue that the proposed methodology is more precise than directly using eq 2. To illustrate this assertion, comparison of the proposed method to eq 2 (dashed line) is plotted in Figure 6 with an example data set for oxygen diffusion in Nafion 211 at 95% RH (open circles). The short-time solution was
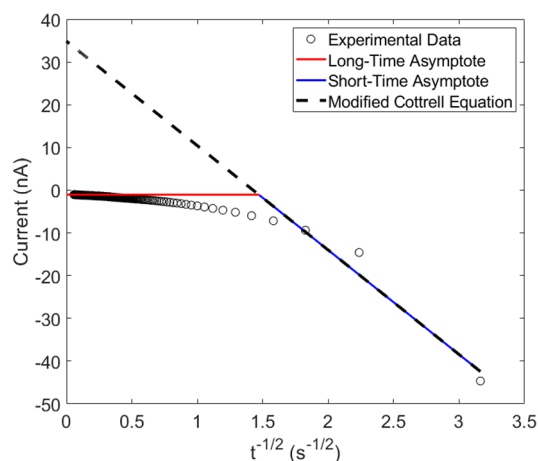
Figure 6. Current versus inverse square root of time with both the short- (blue line) and 2D long-time (red line) asymptotes compared to experimental results (open circles). The modified Cottrell equation (eq 2) is shown as a black dashed line superimposed on the short-time asymptote.

obtained using linear regression and eq 7 (blue line) on the first linear short-time region, whereas eq 6 (red line) was used to calculate the long-time solution. Clearly, the long-time solution fits quite well at long times (>10 s), whereas the short-time solution is only valid for the first four data points (up to ~0.5 s). The diffusivity and Henry's constant calculated from this approach for the data in Figure 6 are quite reasonable, 2.23 × 10^{-12} m^2/s and 208 mol/(m^3·bar), respectively, and the permeability is 4.64 × 10^{-10} mol/(m·bar·s). The standard deviation for the gas permeability is about 5% across multiple samples, while the standard deviations for diffusivity and Henry's constant are approximately 25–30%. This latter error is likely a result of differences in Nafion-membrane samples. Run-to-run variation is less than 5%.

Figure 6 emphasizes the differences between eq 2 and eqs 6 and 7 at long times. The steady-state current calculated using eq 2 fit to the experimental data is positive, which is clearly aphysical for a reduction reaction, further highlighting the importance of eq 6 in fitting the steady-state data. The difference in D, H, and P values that result from the same data set of ORR currents as a function of RH, calculated using both eq 2 and eqs 6 and 7, is given in Section S1.6 and Figure S5 of the Supporting Information. We find that, compared to eq 7, eq 2 produces a diffusivity that is 3 orders of magnitude higher, whereas Henry's constants are 1 order of magnitude lower and the permeability is 2 orders of magnitude higher. These variations are extreme, demonstrating the need for an improved analysis method, as described here, and they reinforce the need for careful data analysis.

Oxygen diffusivity, Henry's constant, and permeability determined from the two-time-regime technique are compared with the results from other studies in Figure 7a–c, respectively, which highlight the wide variability in previously reported works. Differences in temperature (20 versus 40 versus 70 °C) account for some of this variation, but the data from Kudo et al.[22] exhibit higher diffusivity than those of Novitski et al. at a lower temperature. The impact of different membrane processing methods (e.g., Nafion 117 vs 211) on these results is also unclear and may be an additional source of variation in parameter values. In Figure 7, the Novitski (1) data show the results determined by Novitski and Holdcroft using the
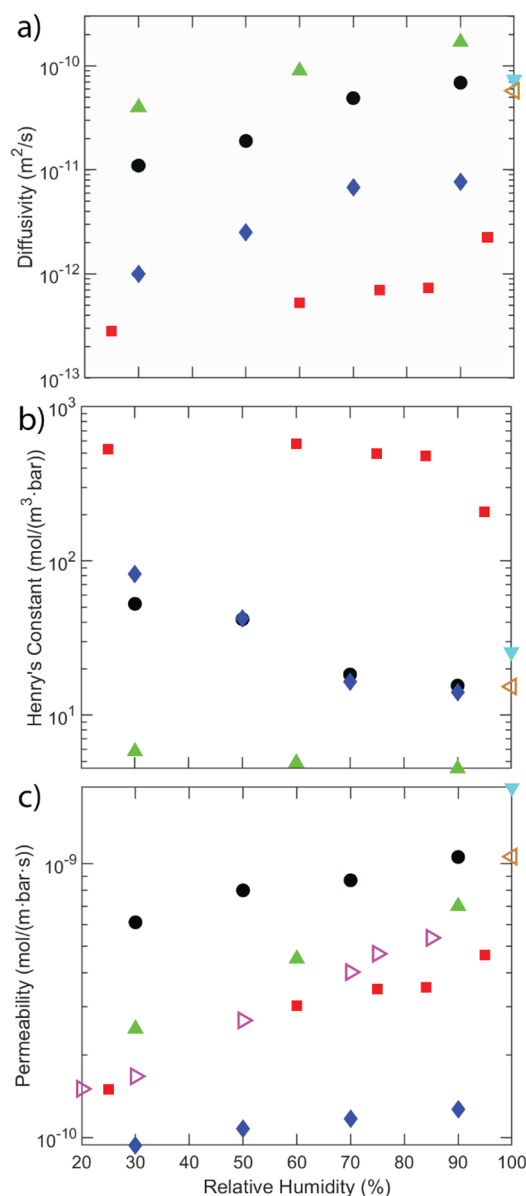

Figure 7. (a) Nafion 211 oxygen diffusivities as a function of relative humidity (red squares) compared with microelectrode literature results [Novitski (1), Nafion 211 (filled black circles), Novitski (2), Nafion 211 (filled blue diamonds), Kudo, 100 μm Nafion, (filled green triangles), and Parthasarathy, Nafion 117 (filled cyan inverted triangles)] and non-microelectrode studies [Baschetti, Nafion 117, (open magenta right triangles) and Sethuraman, Nafion 117, (open brown left triangles)]. (b) Oxygen Henry's constants compared with literature values determined from microelectrode measurements. (c) Oxygen permeabilities compared with the literature determined from microelectrode measurements.[16,17,20–22]

modified Cottrell equation, whereas the Novitski (2) data show the results determined from the Shoup–Szabo equation.[21] These two diffusivities differ by over an order of magnitude depending on the analysis method, further highlighting the importance of an accurate analysis technique. In contrast, Novitski et al. report similar Henry's constants irrespective of the analysis method, thus calculating permeabilities that differ by over an order of magnitude. Results from our work fall between the minimum and maximum reported values for gas permeability but exhibit the lowest diffusivity and

highest Henry's constant values. This is likely the result of two factors. Temperature plays a contributing role as diffusivity typically increases, and Henry's constant decreases at higher temperatures. This study is measured at the lowest reported temperature. In addition, the new proposed analysis technique has a significant impact on reported parameter values compared to the oft-used eq 2, as discussed previously.[1,42,43]

Unlike oxygen, there is a scarcity of data for hydrogen. Measured diffusivity, Henry's constant, and permeability for hydrogen and oxygen in Nafion 211 are given in Figure 8a−c,
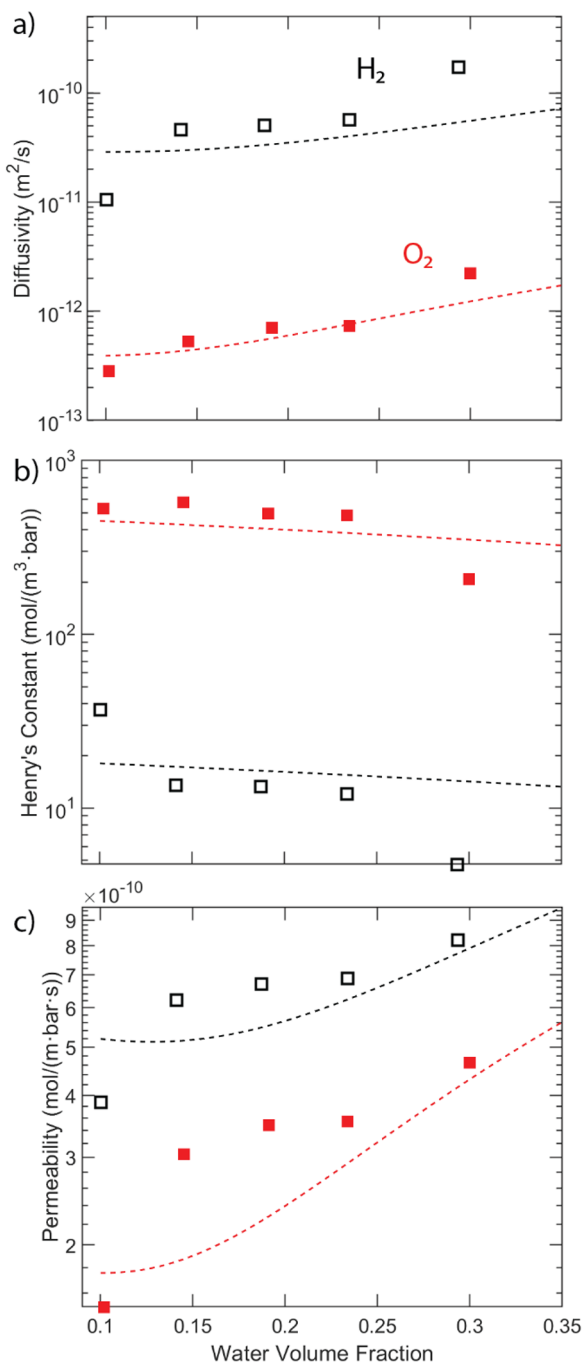

respectively. For oxygen, diffusivity and permeability increase as a function of RH, whereas Henry's constant decreases. This is likely due to the increased size of the aqueous-phase domains at high RH. Oxygen has a higher diffusivity in water than it does in the polymer backbone, but its Henry's constant is lower, as it dissolves more readily in the polymer phase due to interactions with the ether groups in the polymer.[1] Permeability increases because diffusivity increases faster with RH than Henry's constant decreases. These trends are consistent with previous studies of oxygen transport in Nafion membranes, including those not using microelectrodes.[16,21,22,38] Similarly, hydrogen diffusivity increases as the RH increases, whereas hydrogen Henry's constant decreases. This result indicates that hydrogen moves more rapidly through the aqueous phase than through the polymer phase and again dissolves more readily in the polymer phase than in the aqueous phase. Hydrogen permeability, however, still increases overall as RH increases due to the faster increase in diffusivity.

Further insight into the membrane gas-transport processes can be obtained by comparison of the data to the predictions of the parallel phase-separated transport model (eqs 11, 16, and 17), plotted as dashed lines in Figure 8a−c. The water volume fraction was estimated based on tabulated data collected at 25 °C.[1] The values of D and H for hydrogen and oxygen in water were used for the aqueous phase, while dry Nafion was initially used for the polymer phase.[18,44,45] Table 1 lists the parameters used. However, the use of dry Nafion values overestimates the diffusivity and underestimates Henry's constant (with a net underestimation of permeability) by about an order of magnitude (2 orders of magnitude for oxygen Henry's constant). There are a few potential reasons for these discrepancies. It is possible that the membrane is more tortuous than the model calculates, which results in a higher predicted diffusivity than is witnessed experimentally. For Henry's constant, the values measured for dry Nafion are likely lower than the actual values due to some water uptake. It is also difficult to measure gas uptake in a completely dry membrane due to the small Henry's constant. Finally, assumptions used in the model derivation may not strictly hold, such as local equilibrium between the phases, and this contributes to the discrepancy.

To account for potential inaccuracies, effective polymer-phase parameters were used to improve the model fit (effective values found in Table 1). With the effective parameters, the phase separation model is successful at capturing the nonlinearity of the diffusivity, Henry's constant, and permeability as functions of the water volume fraction for both gases, captured in Figure 8. Corresponding plots using the pure polymer-phase parameters can be found in Section S1.7 and Figure S6 in the Supporting Information. Our results demonstrate that treating the aqueous and polymer domains as separate, parallel channels results in qualitative trends consistent with the obtained experimental data, indicating that gas transport occurs predominately through the aqueous phase. However, the lack of quantitative agreement when using the pure polymer-phase parameters likely suggests that the model oversimplifies gas-phase interactions, particularly in the calculation of Henry's constant, as the pure polymer-phase Henry's constant had to be adjusted up to 2 orders of magnitude to achieve a reasonable fit of the experimental data.

Figure 8. (a−c) Diffusivity, Henry's constant, and permeability, respectively, for hydrogen (open squares) and oxygen (filled squares) in Nafion 211. Dashed lines show the theory-predicted values calculated as a function of the water volume fraction using the effective phase-separated parallel-diffusion model.

Table 1. Pure-Phase Transport Parameters for Hydrogen and Oxygen Gas

gas	water[44,45]		dry Nafion[18]	
	diffusivity (m²/s)	Henry's constant(mol/m³·bar)	diffusivity (m²/s)	Henry's constant (mol/m³·bar)
oxygen	2.4×10^{-9}	1.3	5.9×10^{-12}	5.7
hydrogen	6.3×10^{-9}	0.7	1.0×10^{-10}	2.3
oxygen, effective			4.0×10^{-13}	500
hydrogen, effective			3.0×10^{-11}	20

Nafion XL

Figure 9a−c illustrates the gas mass-transport parameters for Nafion XL. Oxygen diffusivity and permeability increase with increasing RH, whereas Henry's constant decreases, similar to Nafion 211. Also, hydrogen diffusivity and permeability increase with increasing RH, whereas Henry's constant decreases, again similar to Nafion 211. These trends occur for the same reasons as they do in Nafion 211, given similarities in their membrane structures. However, diffusivity is generally higher, and Henry's constant is generally lower for both gases in Nafion XL in contrast to Nafion 211, although their product, permeability, is similar in value. This may be a result of the unique structure of Nafion XL, which can be compared to a sandwich—two layers of Nafion, with a polytetrafluoroethylene (PTFE) layer between them.[37] The PTFE layer is highly porous and approximately 2.5 μm thick in an overall membrane thickness of 27.5 μm, with the pores containing additional Nafion ionomer. The added PTFE may produce confinement in the Nafion layers, with chain alignment along the PTFE such that the tortuous water channels are aligned more in the through-plane direction than is found in Nafion 211. This alignment along the PTFE would enhance the through-plane gas diffusivity, the primary diffusivity of interest in this work. Nafion XL is also further modified by the addition of proprietary additives, including possibly silica and cerium, to improve the chemical stability of the membrane.[37,46,47] It is possible that these additives are responsible for some of the differences in diffusivity and solubility seen between Nafion 211 and Nafion XL. Ce is larger than the protons normally found in Nafion and may have widened the water channels in the Nafion such that gas diffusivity is enhanced. In addition, the added concentrations of Ce and silica may have occupied sites where gas would normally dissolve into the membrane, reducing gas dissolution and resulting in the lower observed Henry's constants.

■ CONCLUSIONS

A new method is developed for extracting diffusivity, Henry's constant, and permeability of gases from transient chronoamperometry measurements taken using Pt microelectrodes. A transient 2D numerical model of the microelectrode is implemented. The modified Cottrell equation for data interpretation is supplanted by a two-time-regime analysis: a 2D numerical result at long time and a roughness-corrected Cottrell equation for short time. The new data interpretation methodology is applied to two membranes, Nafion 211 and Nafion XL, to determine the diffusivity, Henry's constant, and permeability of oxygen and hydrogen gases in these membranes as a function of relative humidity (RH). Permeability and diffusivity uniformly increase for all membranes as RH increases, whereas Henry's constant generally decreases as a function of RH. The trends in permeability, diffusivity, and Henry's constant for oxygen in
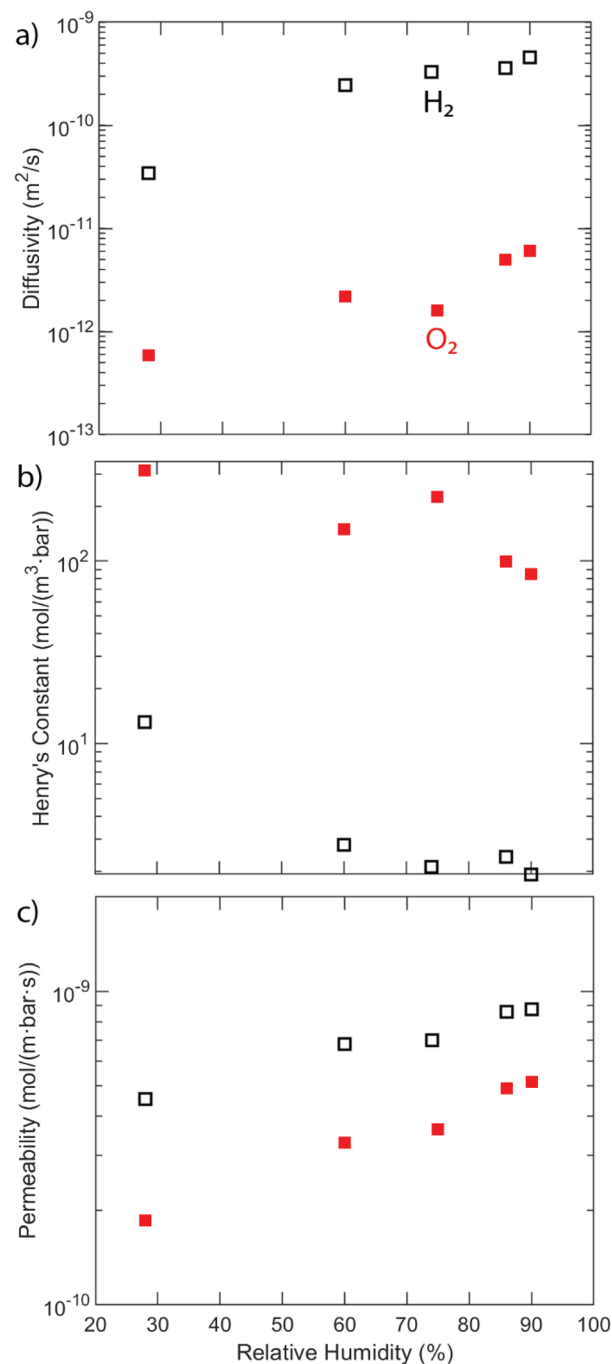

Figure 9. (a−c) Diffusivity, Henry's constant, and permeability, respectively, for hydrogen (open squares) and oxygen (filled squares) in Nafion XL.

Nafion 211 match quite closely with the existing literature but differ quantitatively due to the more rigorous interpretation method applied here, thus highlighting the need to analyze all

data time regimes consistently and holistically and account for such effects as surface roughness. Nafion XL exhibits higher diffusivities, lower Henry's constants, and similar permeabilities for both gases compared to Nafion 211. A phase-separated parallel-diffusion theoretical model also predicts the trends in diffusivity, Henry's constant, and permeability of both hydrogen and oxygen gases in Nafion 211 well when effective polymer-phase properties are used. A more rigorous model may be needed to fit the experimental data quantitatively. Overall, the presented data and methodology suggest that the proposed two-time-regime analysis yields physically reasonable parameters and trends. These findings are important for applications such as determining fuel cell operating conditions, where there is a tradeoff between proton conductivity and gas crossover at high RHs, and precise measurements of gas transport parameters are needed to calculate gas crossover rates. In addition, this study highlights how to use and interpret solid-state microelectrodes effectively and rigorously for mass-transport interrogations.

ASSOCIATED CONTENT

Supporting Information

The Supporting Information is available free of charge at https://pubs.acs.org/doi/10.1021/acsmeasuresciau.1c00058.

> Nafion structure, calculating the ECSA from CVs, polarization curves, numerics, microelectrode surface AFM, comparison of the modified Cottrell equation with this work, unadjusted phase-separated parallel-diffusion model, and error bar analysis (PDF)

AUTHOR INFORMATION

Corresponding Author

Adam Z. Weber — *Energy Conversion Group, Energy Technologies Area, Lawrence Berkeley National Laboratory, Berkeley, California 94720, United States;* ⓘ orcid.org/0000-0002-7749-1624; Phone: (510) 486-6308; Email: azweber@lbl.gov; Fax: (510) 486-7303

Authors

John G. Petrovick — *Department of Chemical and Biomolecular Engineering, University of California, Berkeley, California 94720, United States; Energy Conversion Group, Energy Technologies Area, Lawrence Berkeley National Laboratory, Berkeley, California 94720, United States*

Clayton J. Radke — *Department of Chemical and Biomolecular Engineering, University of California, Berkeley, California 94720, United States;* ⓘ orcid.org/0000-0002-1587-4822

Complete contact information is available at:
https://pubs.acs.org/10.1021/acsmeasuresciau.1c00058

Author Contributions

All authors have given approval to the final version of the manuscript.

Notes

The authors declare no competing financial interest.

ACKNOWLEDGMENTS

ABBREVIATIONS

PEFC   polymer-electrolyte fuel cell
HOR   hydrogen oxidation reaction
ORR   oxygen reduction reaction
Pt   platinum
PFSA   perfluorinated sulfonic acid
EW   equivalent weight
RDE   rotating disk electrode
RHE   reversible hydrogen electrode
PEEK   polyether ether ketone
GDE   gas diffusion electrode
AFM   atomic force microscopy
CV   cyclic voltammetry
ECSA   electrochemical surface area
RH   relative humidity
OCV   open-circuit voltage

REFERENCES

(1) Kusoglu, A.; Weber, A. Z. New Insights into Perfluorinated Sulfonic-Acid Ionomers. *Chem. Rev.* **2017**, *117*, 987−1104.

(2) Rodgers, M. P.; Bonville, L. J.; Kunz, H. R.; Slattery, D. K.; Fenton, J. M. Fuel cell perfluorinated sulfonic acid membrane degradation correlating accelerated stress testing and lifetime. *Chem. Rev.* **2012**, *112*, 6075−6103.

(3) Holdcroft, S. Fuel Cell Catalyst Layers: A Polymer Science Perspective. *Chem. Mater.* **2014**, *26*, 381−393.

(4) Weber, A. Z.; Kusoglu, A. Unexplained transport resistances for low-loaded fuel-cell catalyst layers. *J. Mater. Chem. A* **2014**, *2*, 17207−17211.

(5) Bird, R. B.; Stewart, W. E.; Lightfoot, E. N., *Transport Phenomena*. rev. 2nd ed.; John Wiley & Sons, Inc.: New York, 2007.

(6) Cullen, D. A.; Neyerlin, K. C.; Ahluwalia, R. K.; Mukundan, R.; More, K. L.; Borup, R. L.; Weber, A. Z.; Myers, D. J.; Kusoglu, A. New roads and challenges for fuel cells in heavy-duty transportation. *Nat. Energy* **2021**, *6*, 462−474.

(7) Borup, R.; Meyers, J.; Pivovar, B.; Kim, Y. S.; Mukundan, R.; Garland, N.; Myers, D.; Wilson, M.; Garzon, F.; Wood, D.; Zelenay, P.; More, K.; Stroh, K.; Zawodzinski, T.; Boncella, J.; McGrath, J. E.; Inaba, M.; Miyatake, K.; Hori, M.; Ota, K.; Ogumi, Z.; Miyata, S.; Nishikata, A.; Siroma, Z.; Uchimoto, Y.; Yasuda, K.; Kimijima, K.; Iwashita, N. Scientific aspects of polymer electrolyte fuel cell durability and degradation. *Chem. Rev.* **2007**, *107*, 3904−3951.

(8) Borup, R. L.; Kusoglu, A.; Neyerlin, K. C.; Mukundan, R.; Ahluwalia, R. K.; Cullen, D. A.; More, K. L.; Weber, A. Z.; Myers, D. J. Recent developments in catalyst-related PEM fuel cell durability. *Curr. Opin. Electrochem.* **2020**, *21*, 192−200.

(9) Gierke, T. D.; Hsu, W. Y. The Cluster-Network Model of Ion Clustering in Perfluorosulfonated Membranes. *Acs Sym Ser* **1982**, *180*, 283−307.

(10) Kreuer, K.-D.; Portale, G. A Critical Revision of the Nano-Morphology of Proton Conducting Ionomers and Polyelectrolytes for Fuel Cell Applications. *Adv. Funct. Mater.* **2013**, *23*, 5390−5397.

(11) Mauritz, K. A.; Moore, R. B. State of understanding of nafion. *Chem. Rev.* **2004**, *104*, 4535−4586.

(12) Wood, D. L., III; Chlistunoff, J.; Majewski, J.; Borup, R. L. Nafion Structural Phenomena at Platinum and Carbon Interfaces. *J. Am. Chem. Soc.* **2009**, *131*, 18096−18104.

(13) White, H. S.; Leddy, J.; Bard, A. J. Polymer Films on Electrodes. 8. Investiagtion of Charge-Transport Mechanisms in Nafion Polymer Electrodes. *J. Am. Chem. Soc.* **1982**, *104*, 4811−4817.

(14) Zook, L. A.; Leddy, J. Density and solubility of nafion: recast, annealed, and commercial films. *Anal. Chem.* **1996**, *68*, 3793−3796.

(15) Tesfaye, M.; MacDonald, A. N.; Dudenas, P. J.; Kusoglu, A.; Weber, A. Z. Exploring substrate/ionomer interaction under oxidizing and reducing environments. *Electrochem. Commun.* **2018**, *87*, 86−90.

(16) Giacinti Baschetti, M.; Minelli, M.; Catalano, J.; Sarti, G. C. Gas permeation in perflurosulfonated membranes: Influence of temperature and relative humidity. *Int. J. Hydrogen Energy* **2013**, *38*, 11973−11982.

(17) Sethuraman, V. A.; Khan, S.; Jur, J. S.; Haug, A. T.; Weidner, J. W. Measuring Oxygen, Carbon Monoxide and Hydrogen Sulfide Diffusion Coefficient and Solubility in Nafion Membranes. *Electrochim. Acta* **2009**, *54*, 6850−6860.

(18) Mukaddam, M.; Litwiller, E.; Pinnau, I. Gas Sorption, Diffusion, and Permeation in Nafion. *Macromolecules* **2016**, *49*, 280−286.

(19) Broka, K.; Ekdunge, P. Oxygen and hydrogen permeation properties and water uptake of Nafion(R) 117 membrane and recast film for PEM fuel cell. *J. Appl. Electrochem.* **1997**, *27*, 117−123.

(20) Parthasarathy, A.; Martin, C. R.; Srinivasan, S. Investigations of the O2 Reduction Reaction at the Platinum/Nafion® Interface Using a Solid-State Electrochemical Cell. *J. Electrochem. Soc.* **1991**, *138*, 916−921.

(21) Novitski, D.; Holdcroft, S. Determination of O(2) Mass Transport at the Pt | PFSA Ionomer Interface under Reduced Relative Humidity. *ACS Appl. Mater. Interfaces* **2015**, *7*, 27314−27323.

(22) Kudo, K.; Jinnouchi, R.; Morimoto, Y. Humidity and Temperature Dependences of Oxygen Transport Resistance of Nafion Thin Film on Platinum Electrode. *Electrochim. Acta* **2016**, *209*, 682−690.

(23) Mohamed, H. F. M.; Ito, K.; Kobayashi, Y.; Takimoto, N.; Takeoka, Y.; Ohira, A. Free volume and permeabilities of O2 and H2 in Nafion membranes for polymer electrolyte fuel cells. *Polymer* **2008**, *49*, 3091−3097.

(24) Cheng, X.; Zhang, J.; Tang, Y.; Song, C.; Shen, J.; Song, D.; Zhang, J. Hydrogen crossover in high-temperature PEM fuel cells. *J. Power Sources* **2007**, *167*, 25−31.

(25) Zhang, Z.; Chattot, R.; Bonorand, L.; Jetsrisuparb, K.; Buchmüller, Y.; Wokaun, A.; Gubler, L. Mass spectrometry to quantify and compare the gas barrier properties of radiation grafted membranes and Nafion®. *J. Membr. Sci.* **2014**, *472*, 55−66.

(26) Sakai, T.; Takenaka, H.; Torikai, E. Gas Diffusion in the Dried and Hydrated Nations. *J. Electrochem. Soc.* **1986**, *133*, 88−92.

(27) Bard, A. J.; Faulkner, L. R., *Electrochemical Methods: Fundamentals and Applications.* 2nd ed.; John Wiley & Sons, Inc.: New York, 2001.

(28) Petrovick, J. G.; Anderson, G.; Kushner, D. I.; Danilovic, N.; Weber, A. Z. Methods—Using Microelectrodes to Explore Solid Polymer Electrolytes. *J. Electrochem. Soc.* **2021**, No. 056517.

(29) Bond, A. M.; Oldham, K. B.; Zoski, C. G. Theory of Electrochemical Processes at an Inlaid Disc Microelectrode Under Steady-State Conditions. *J. Electroanal. Chem.* **1988**, *245*, 71−104.

(30) Parthasarathy, A.; Davé, B.; Srinivasan, S.; Appleby, A. J.; Martin, C. R. The Platinum Microelectrode/Nafion Interface: An Electrochemical Impedance Spectroscopic Analysis of Oxygen Reduction Kinetics and Nafion Characteristics. *J. Electrochem. Soc.* **1992**, *139*, 1634.

(31) Novitski, D.; Kosakian, A.; Weissbach, T.; Secanell, M.; Holdcroft, S. Electrochemical Reduction of Dissolved Oxygen in Alkaline, Solid Polymer Electrolyte Films. *J. Am. Chem. Soc.* **2016**, *138*, 15465−15472.

(32) Peron, J.; Mani, A.; Zhao, X.; Edwards, D.; Adachi, M.; Soboleva, T.; Shi, Z.; Xie, Z.; Navessin, T.; Holdcroft, S. Properties of Nafion® NR-211 membranes for PEMFCs. *J. Membr. Sci.* **2010**, *356*, 44−51.

(33) Büchi, F. N.; Wakizoe, M.; Srinivasan, S. Microelectrode Investigation of Oxygen Permeation in Perfluorinated Proton Exchange Membranes with Different Equivalent Weights. *J. Electrochem. Soc.* **1996**, *143*, 927.

(34) Basura, V. I.; Chuy, C.; Beattie, P. D.; Holdcroft, S. Effect of equivalent weight on electrochemical mass transport properties of oxygen in proton exchange membranes based on sulfonated a,b,b-trifluorostyrene (BAM ®) and sulfonated styrene-(ethylene-butylene)-styrene triblock (DAIS-analytical) copolymers. *J. Electroanal. Chem.* **2001**, *501*, 77−88.

(35) Chlistunoff, J. Oxygen permeability of cast ionomer films from chronoamperometry on microelectrodes. *J. Power Sources* **2014**, *245*, 203−207.

(36) Petrovick, J. G.; Kushner, D. I.; Tesfaye, M.; Danilovic, N.; Radke, C. J.; Weber, A. Z. Mass-Transport Resistances of Acid and Alkaline Ionomer Layers: A Microelectrode Study Part 1 - Microelectrode Development. *ECS Trans.* **2019**, *92*, 77−85.

(37) Shi, S.; Weber, A. Z.; Kusoglu, A. Structure/property relationship of Nafion XL composite membranes. *J. Membr. Sci.* **2016**, *516*, 123−134.

(38) Evans, C. M.; Singh, M. R.; Lynd, N. A.; Segalman, R. A. Improving the Gas Barrier Properties of Nafion via Thermal Annealing: Evidence for Diffusion through Hydrophilic Channels and Matrix. *Macromolecules* **2015**, *48*, 3303−3309.

(39) Crothers, A. R.; Radke, C. J.; Weber, A. Z. Impact of Nano- and Mesoscales on Macroscopic Cation Conductivity in Perfluorinated-Sulfonic-Acid Membranes. *J. Phys. Chem. C* **2017**, *121*, 28262−28274.

(40) Yasuda, H.; Lamaze, C. E.; Peterlin, A. Diffusive and Hydraulic Permeabilities of Water in Water-Swollen Polymer Membranes. *J. Polym. Sci., Part A-2: Polym. Phys.* **1971**, *9*, 1117−1131.

(41) Currie, J. A. Gaseous diffusion in porous media. Part 2.-Dry granular materials. *Br. J. Appl. Phys.* **1960**, *11*, 318.

(42) Beattie, P. D.; Basura, V. I.; Holdcroft, S. Temperature and pressure dependence of O$_2$ reduction at Pt|Nafion® 117 and Pt|BAM® 407 interfaces. *J. Electroanal. Chem.* **1999**, *468*, 180−192.

(43) Parthasarathy, A.; Srinivasan, S.; Appleby, A. J.; Martin, C. R. Temperature-Dependence of the Electrode-Kinetics of Oxygen Reduction at the Platinum Nafion(R) Interface - a Microelectrode Investigation. *J. Electrochem. Soc.* **1992**, *139*, 2530−2537.

(44) Bergman, T. L.; Lavine, A. S.; Incropera, F. P.; Dewitt, D. P., *Fundamentals of Heat and Mass Transfer.* Seventh ed.; John Wiley & Sons, Inc.: Hoboken, NJ, 2011.

(45) Sander, R. Compilation of Henry's law constants (version 4.0) for water as solvent. *Atmos. Chem. Phys.* **2015**, *15*, 4399−4981.

(46) Stewart, S. M.; Spernjak, D.; Borup, R.; Datye, A.; Garzon, F. Cerium Migration through Hydrogen Fuel Cells during Accelerated Stress Testing. *ECS Electrochem. Lett.* **2014**, *3*, F19−F22.

(47) Danilczuk, M.; Schlick, S.; Coms, F. D. Cerium(III) as a Stabilizer of Perfluorinated Membranes Used in Fuel Cells: In Situ Detection of Early Events in the ESR Resonator. *Macromolecules* **2009**, *42*, 8943−8949.